Available online at www.sciencedirect.com
SCIENCE DIRECT
Journal of Catalysis 240 (2006) 222–234
JOURNAL OF CATALYSIS
www.elsevier.com/locate/jcat

The effect of gold particle size on Au–Au bond length and reactivity toward oxygen in supported catalysts

J.T. Miller [a,*], A.J. Kropf [b], Y. Zha [c], J.R. Regalbuto [c], L. Delannoy [d], C. Louis [d], E. Bus [e], J.A. van Bokhoven [e]

[a] *BP Research Center, 150 W. Warrenville Road, Naperville, IL 60565-8406, USA*
[b] *Argonne National Laboratory, Chemical Engineering Division, Argonne, IL 60439, USA*
[c] *University of Illinois at Chicago, Department of Chemical Engineering, Chicago, IL 60607, USA*
[d] *Laboratoire de Réactivité de Surface, UMR 7609 CNRS, Université Pierre et Marie Curie, 4 place Jussieu, 75252, Paris cedex 05, France*
[e] *Institute for Chemical and Bioengineering, Swiss Federal Institute of Technology, ETH, CH-8093, Zurich, Switzerland*

Received 6 January 2006; revised 3 April 2006; accepted 4 April 2006

Abstract

Au catalysts with different metallic particle sizes and supported on silica, alumina, titania, zirconia, ceria, and niobia were prepared, and the reduced catalysts were characterized by EXAFS spectroscopy. As the Au–Au coordination number decreased, the interatomic bond length decreased. The Au–Au bond length contraction appears to be independent of the support type. A correlation between the dispersion of Pt catalysts determined by hydrogen chemisorption and the EXAFS Pt–Pt coordination number was established and used to determine the dispersion of fully reduced Au catalysts. In addition, the Au particle size was estimated using a literature correlation of the EXAFS coordination number. For particles larger than about 40 Å, there was little change in the metallic bond length, whereas in catalysts with gold particles smaller than 30 Å, the Au–Au distance decreased with decreasing particle size, with a maximum contraction of about 0.15 Å. Decreasing particle size also brought a decrease in the intensity of the white line of the XANES spectrum. Both the decrease in bond distance and white line intensity were consistent with an increase in the d-electron density of Au atoms in very small particles. Au particles smaller than about 30 Å were also reactive to air, leading to oxidation of up to 15% of the atoms of the gold particles, depending on the size; larger particles were not oxidized. These oxidized Au atoms in small particles are suggested to be active for CO oxidation.

Keywords: Au EXAFS; Au XANES; Au catalysts; Au catalyst preparation; Au bond length contraction; Au on alumina; Au on titania; Au on ceria; Au on silica; Au on zirconia; Au on niobia; Pt EXAFS; Au dispersion from EXAFS; Particle size effect in Au catalysts

1. Introduction

Early reviews indicated that gold is catalytic for hydrogen–deuterium exchange, olefin hydrogenation, NO_x reduction with H_2, paraffin skeletal isomerization, and partial oxidation, although the activity was generally considered very low compared with other metals [1–6]. As a result, for many years gold catalysts received relatively little attention compared with group VIII and other transition metal catalysts. The discovery in 1987 that supported Au catalysts with small gold particles are highly active for CO oxidation at temperatures lower than those typical of Pt catalysts [7–10] sparked a greatly increased interest in Au catalysts. Several excellent reviews on the development and characterization of Au catalysts have been published recently [11–18].

Various explanations have been advanced to account for the high activity in Au catalysts. Although there is general agreement that the activity of Au increases as the size of the metal particle decreases below about 50 Å (and especially below about 30 Å) [8–10,19–29], the enhanced activity is suggested to be due to very small (metallic) particles [23], ensembles of partially oxidized and metallic sites [30,31], anionic gold clusters [32,33], or cationic Au [34,35]. For CO oxidation, the role

* Corresponding author.
E-mail address: millejt1@bp.com (J.T. Miller).

0021-9517/$ – see front matter
doi:10.1016/j.jcat.2006.04.004

of the support is also thought to be essential to high activity [8–11,30]. Generally, Au on TiO_2 and Fe_2O_3 are the most active catalysts [8–11,24]. Whereas CO adsorbs on low-coordination sites, the activation of O_2 is unclear, because oxygen does not adsorb on metallic Au at low temperatures. Thus, it has been suggested that the O_2 activation occurs at the metal–support interface [36,37] or on reducible supports providing activated oxygen for reaction [8–11,19,21].

As metal particles become smaller, not only does the fraction of surface sites increase, but also other changes in the metallic properties occur; for example, the FCC structure of bulk gold transforms into decahedral or icosahedral particles when particles are very small. Cleveland et al. [38] predicted that transition from bulk FCC to decahedral occurs for particles smaller than about 200 atoms (ca. 25 Å) and to icosahedral particles smaller than 100 atoms (ca. 16 Å). Uppenbrink and Wales [39] found that the transition from FCC to icosahedral occurs for particles smaller than 550 atoms. Experimentally, 50-Å Pt particles on carbon have a cubo-octahedral shape [40], whereas 10-Å particles on Y zeolite have icosahedral symmetry [41].

In general, as the size of metal particles decreases, the metal–metal bond length tends to decrease. Overall, there is good agreement using several techniques, indicating that in thin films and unsupported metal Cr, Fe, Cu, Ag, Pd, Au, and Pt particles smaller than about 30 Å, a shortening of the interatomic bond distance occurs [42–53]. For example, in 31-Å Ag particles deposited by vacuum evaporation on cellulose, there was a 2.7% contraction in the bond distance determined by electron diffraction [42]. As the particle size decreases, the interatomic distance decreases more significantly. The bond distance of Au evaporated on Mylar was determined by EXAFS [48,49,51]; a 30-Å particle had a bond distance of 2.84 Å (a contraction of about 1.4%), whereas an 8-Å particle had a bond distance of 2.72 Å, 5.5% shorter than that in Au foil (2.88 Å). The contraction of the interatomic bond distance determined by EXAFS is even more pronounced for dimeric Fe particles cryogenically deposited in a dilute Ne matrix, for example, a bond length of 2.02 Å compared with 2.48 Å, or a contraction of 18.5% in α-Fe [44]. Similarly, in dimeric Ag, the metal–metal distance is 2.47 Å, compared with 2.89 Å for bulk Ag [54].

Substantial bond length contractions of the bond distance have also been reported for small metal particles on weakly interacting supports such as carbon. For both Cu and Ni on carbon, as the particle size decreased below about 40 Å, the bond distance decreased by about 10% (ca. 0.2 Å) compared with the bulk distance [55,56]. Evaporated Pt particles deposited on thin alumina films under vacuum exhibited a contraction of about 10% for particles smaller than 10 Å [52].

In addition to a contraction in the metallic bond length, changes in the electronic, magnetic, and chemical properties were observed on Cu, Ag, Au, and Pt as the thickness of the metal film, or particles, decreased to a few nanometers [57–64]. Electron energy loss spectroscopy (EELS) and X-ray photoelectron spectroscopy (XPS) analysis of the Cu particles indicated a shift of the d-band toward isolated atoms with decreasing particle size [60]. Similar shifts in the energy of the valence and core-level orbitals have been observed in small Pt and Pd particles supported on carbon [59]. Changes in the photoemission spectra are also indicative of changes in the d-band splitting and changes in the local density of states near the Fermi level for carbon-supported Au particles smaller than about 19 Å; however, for larger particles, the spectra are similar to bulk foil [61]. Similarly, 14 Å Au particles on carbon supports displayed a 0.45-eV shift in the XPS spectra, whereas 60 Å Au particles were identical to Au foil [65]. Using scanning tunneling spectroscopy (STS), 3-nm two-dimensional Au particles (or about 200 atoms) supported on TiO_2(110) exhibited a band gap of 0.2–0.6 eV, and thus were less metallic than bulk Au [23]. These 3-nm particles also displayed the highest turnover rate. The high CO oxidation activity was suggested to be due to a quantum size effect, that is, a transition from metal to nonmetal or semiconductor properties. Although small particles may exhibit electronic changes, monolayer islands of gold (one or two layers in height) supported on FeO(111) have been shown to not adsorb CO differently than larger three-dimensional particles [66]. The high activity of small particles was thought to be due to the large fraction of coordinatively unsaturated surface atoms rather than to a quantum size effect.

In this study, Au nanoparticles on different oxide supports are synthesized with different sizes and characterized by XAFS spectroscopy. Using a correlation between hydrogen chemisorption and the EXAFS coordination number for Pt catalysts, the dispersion of the Au particles is estimated from the Au–Au coordination number. As the dispersion increases or the particle size decreases, the metallic bond length decreases. In addition, as the size of the Au particles decreases, the intensity of the white line of the XANES spectra decreases. Finally, on the smallest particles, about 10% of the metallic Au atoms are oxidized by air, giving Au^{III}–O surface sites that are suggested to be active for CO oxidation.

2. Experimental

2.1. Pt catalyst preparation

2.1.1. 2.0% Pt on silica by dry impregnation (DI)

A 0.90-g sample of $Pt(NH_3)_4(NO_3)_2$ in 45 mL of H_2O was added to 45 g of silica (Davisil 644, 290 m^2/g and 1.16 cc/g). The initial pH of the PTA solutions was about 5.0. After 4 h, the catalyst was dried overnight at 100 °C in a forced-air, ventilated oven. The Pt elemental analysis determined by ICP was 2.03 wt%.

2.1.2. 2.0% Pt on silica by strong electrostatic adsorption (SEA)

A 45-g silica sample was slurried in 400 mL of H_2O. The pH was increased to 9.5 by adding concentrated NH_4OH. Then 0.90 g of $Pt(NH_3)_4(NO_3)_2$ dissolved in 50 mL of H_2O was added. After 1 h, the solid was filtered and washed twice with 250 mL of H_2O and dried overnight at 100 °C. The Pt elemental analysis determined by ICP was 2.06 wt% and indicated that virtually all of the PTA in solution had been adsorbed.

Table 1
2% Pt catalysts prepared from $Pt(NH_3)_4(NO_3)_2$ (PTA), method of preparation, calcination temperature before reduction at 250 °C and dispersion

Sample ID	Support[a]	Method	Calcination temperature (°C)	% Dispersion[b]
Pt-Si1	SiO_2	DI[c]	100	63
Pt-Si2	SiO_2	DI	100	51
Pt-Si3	SiO_2	DI	225	29
Pt-Si4	SiO_2	DI	250	29
Pt-Si5	SiO_2	DI	250	32
Pt-Si6	SiO_2	DI	525	24
Pt-Si7	SiO_2	SEA	100	79
Pt-Si8	SiO_2	SEA	200	96
Pt-Si9	SiO_2	SEA	225	100
Pt-Si10	SiO_2	SEA	400	41
Pt-Si11	SiO_2	SEA	500	24
Pt-Si12	SiO_2	SEA	550	19
Pt-Si13	SiO_2	SEA	600	11
Pt-Al1	Al_2O_3	DI	250	81
Pt-Al2	Al_2O_3	DI[d]	500	81
Pt-Al3	Al_2O_3	DI[e]	500	82
Pt-Al4	Al_2O_3	DI	500	70
Pt-Al5	Al_2O_3	DI	550	57
Pt-Al6	Al_2O_3	DI	580	30
Pt-Al7	Al_2O_3	DI	625	18

[a] Silica (290 m^2/g and 1.16 cc/g); alumina calcined at 700 °C (165 m^2/g and 0.49 cc/g).
[b] Determined by hydrogen chemisorption after reduction at 250 °C for 1 h.
[c] DI at pH of 10 by addition of NH_4OH.
[d] Alumina calcined at 500 °C (225 m^2/g and 0.38 cc/g).
[e] DI with H_2PtCl_6 at a pH of 3 with alumina calcined at 500 °C.

The DI and SEA Pt/silica catalysts were calcined in flowing air at 100–600 °C to alter the dispersion. The temperature was increased at 1 °C/min to the final temperature and maintained at that temperature for 3 h. After calcination, 10 g of catalyst was reduced at atmospheric pressure in flowing H_2 (200 cc/min) by heating from room temperature to 250 °C at a rate of 5 °C/min and holding there for 2 h [67].

2.1.3. 2.0% Pt on alumina by DI

To 50 g of Catapal alumina calcined at 700 °C (165 m^2/g and 0.49 cc/g) was added 1.50 g $Pt(NH_3)_4(NO_3)_2$ in 40 mL and dried at 100 °C. The Pt elemental analysis determined by ICP was 1.95 wt%. The catalysts were calcined at 250–625 °C to alter the dispersion and reduced at 250 °C.

The hydrogen chemisorption capacity was determined on the reduced Pt catalysts by the double-isotherm method using a Coulter Omnisorb 100CX instrument. The previously reduced catalyst was re-reduced for 1 h and evacuated for 1 h at 250 °C, then cooled to room temperature in vacuum. The first isotherm was determined at room temperature; then the sample was evacuated at room temperature, and the second H_2 isotherm was determined. The hydrogen chemisorption capacity was determined by the difference in the two isotherms extrapolated to zero pressure and assuming a hydrogen atom-to-surface Pt stoichiometry of 1.0. The Pt catalyst IDs, compositions, method of preparation, and percent dispersions are given in Table 1.

2.2. Au catalyst preparation

Au catalysts were prepared by adding $HAuCl_4$ to alumina (Catapal, 220 m^2/g and 0.39 mL/g and Versal GH, 225 m^2/g and 1.0 mL/g), silica (XOA400, 400 m^2/g, 2.1 mL/g), titania (P25 Degussa, 45 m^2/g, 0.6 mL/g), ceria, zirconia (MEI, 22 m^2/g and 0.61 mL/g), and niobia (CBMM, 160 m^2/g and 0.64 mL/g, and 20 m^2/g and 0.55 mL/g) by several methods. Cerium oxide was prepared by calcination of $Ce(C_2H_3O_2)_3 \cdot xH_2O$ (Aldrich) at 425 °C for 24 h (80 m^2/g and 0.14 mL/g).

2.2.1. Preparation by SEA

To 50.0 g of Catapal γ-alumina in 500 mL H_2O was added 1.53 g $HAuCl_4$ dissolved in 200 mL of cold H_2O. The pH of the solution was approximately 3. The solution was stirred for 1 h, filtered, and washed with 500 mL of H_2O, filtered, and dried overnight at 100 °C. The elemental analysis was 1.38 wt% Au and 0.90 wt% Cl, respectively. The amount of $HAuCl_4$ was adjusted to give catalysts with other Au loadings (Table 2).

2.2.2. Removal of Cl ions by addition of NaOH

A 35-g sample of 1.38 wt% Au (0.9 wt% Cl) on alumina (catalyst from above) was slurried in 200 mL of H_2O and heated to about 70 °C. A solution of NaOH (pH = 13) was added dropwise to maintain a pH of 7–9. The solution was stirred until the pH remained at 9. The solid was filtered, washed with 100 mL of H_2O, filtered again, and dried overnight at 100 °C. The elemental analysis was 1.02 wt% Au and <0.01 wt% Cl and 0.01 wt% Na (Table 2).

2.2.3. Au on other supports by SEA

Additional catalysts were prepared on Versal alumina, P25 titania, ceria, zirconia, and high- and low-surface area niobia. Gold was adsorbed using the mass of oxide to provide 500 m^2/L of oxide in 40 mL of 290 ppm $HAuCl_4$ solution with an initial pH of 3.1 (natural pH). Gold was also adsorbed at an initial pH of about 6 by the addition of NaOH. After 1 h, the catalysts were filtered and dried overnight at 100 °C in flowing air. No attempts were made to remove residual Cl. The final solution pH, Au and Cl concentrations are given in Table 2.

2.2.4. 0.7 and 3.5 wt% Au/support by deposition-precipitation with urea (DPU)

A solution of $HAuCl_4$ was prepared by dissolving the appropriate amount of $HAuCl_4 \cdot 3H_2O$ in 100 mL of deionized water. Then 1 g of support and urea (concentration $100 \times C$) was added, and the suspension was stirred and heated to 80 °C for 16 h in a closed reactor to eliminate exposure to light. Then the solid was centrifuged, washed three times with deionized water, and dried under vacuum at room temperature for 2 h [68,69].

2.2.5. 0.7 and 3.5 wt% Au/support by incipient wetness impregnation

The support was impregnated with an aqueous solution of $HAuCl_4$; the pH of the solution pH was <1. The samples were aged at room temperature for 1 h, then washed twice with

Table 2
Au catalyst composition and method of preparation

Sample ID	Support	Au (wt%)	Method[a]	pH	Cl removal	Reduction temperature (°C)
Au-Si1	SiO_2	2.37 <200 ppm Cl	IMPN	<1	NH_3	175
Au-Si2	SiO_2	3.17 <200 ppm Cl	IMPN	<1	NH_3	250
Au-Al1	Al_2O_3	0.94 1.7 wt% Cl	SEA	4	None	250
Au-Al2	Al_2O_3	1.38 0.9 wt% Cl	SEA	3	None	250
Au-Al3	Al_2O_3	0.58 20 ppm Cl	SEA	4	NaOH	250
Au-A44	Al_2O_3	1.02 38 ppm Cl	SEA	4	NaOH	250
Au-Al5	Al_2O_3	1.31 20 ppm Cl	SEA	3	NaOH	250
Au-Al6	Al_2O_3	1.5 <200 ppm Cl	SEA	4	None	250
Au-Al7	Al_2O_3	2.3 0.81% Cl	SEA	6	None	250
Au-Ti1	TiO_2	2.89 350 ppm Cl	DPN	8	H_2O	175
Au-Ti2	TiO_2	2.41 <200 ppm Cl	IMPN	<1	NH_3	175
Au-Ti3	TiO_2	3.27 <200 ppm Cl	IMPN	<1	NH_3	175
Au-Ti4	TiO_2	0.62 <200 ppm Cl	IMPN	<1	NH_3	200
Au-Ti5	TiO_2	0.58 <200 ppm Cl	DPU	2.5–7	H_2O	200
Au-Ti6	TiO_2	3.56 <200 ppm Cl	DPU	2.5–7	H_2O	250
Au-Ti7	TiO_2	3.56 <200 ppm Cl	DPU	2.5–7	H_2O	250
Au-Ti8	TiO_2	1.4 1.4% Cl	SEA	3	None	250
Au-Ti9	TiO_2	3.6 0.8% Cl	SEA	6	None	250
Au-Ce1	CeO_2	3.37 <200 ppm Cl	DPU	2.5–7	H_2O	250
Au-Ce2	CeO_2	0.47 <200 ppm Cl	DPU	2.5–7	H_2O	200
Au-Ce3	CeO_2	3.8 0.11% Cl	SEA	7	None	250
Au-Nb1	Nb_2O_5	2.1 1.3% Cl	SEA	5	None	150
Au-Nb2	Nb_2O_5	2.5 2.2% Cl	SEA	5	None	250
Au-Zr1	ZrO_2	2.0 1.0% Cl	SEA	6	None	250

[a] Catalysts dried at 100 °C prior to reduction.

an aqueous ammonia solution (1 M, pH 11) and twice with deionized water, with centrifugation between each washing. The samples were dried under vacuum at room temperature for 2 h.

2.2.6. 3 wt% Au/support by DPN

A solution of $HAuCl_4$ (4.2×10^{-3} M) was prepared by dissolving the appropriate amount of $HAuCl_4 \cdot 3H_2O$ in 100 mL of deionized water. The solution was heated to 80 °C, and the pH was adjusted to 8 by dropwise addition of NaOH (1 M); then 1 g of support was dispersed in the solution, and the pH was readjusted to 8 with NaOH. The suspension was stirred at 80 °C for 1 h. Then the solid was centrifuged, washed three times with deionized water, and dried under vacuum at room temperature for 2 h [68,69].

The Au catalyst sample designations, compositions, and methods of preparation are given in Table 2.

2.3. EXAFS and XANES data collection and analysis

X-Ray absorption measurements were made on the insertion device beamline of the Materials Research Collaborative Access Team (MRCAT) at the Advanced Photon Source, Argonne National Laboratory. A cryogenically cooled double-crystal Si(111) monochromator was used in conjunction with an uncoated glass mirror, to minimize the presence of harmonics. The monochromator was scanned continuously during the measurements, with data points integrated over 0.5 eV for 0.07 s per data point. Measurements were made in transmission mode with the ionization chambers optimized for the maximum current with linear response ($\sim 10^{10}$ photons detected/s) using a mixture of nitrogen and helium in the incident X-ray detector and a mixture of ca. 20% argon in nitrogen in the transmission X-ray detector. A gold foil spectrum was acquired simultaneously with each measurement for energy calibration.

Dried catalyst samples were pressed into a cylindrical holder with a thickness chosen to give a total absorbance (μx) at the Au L_{III} (and Pt L_{III}) edge of about 3.0 and a gold edge step ($\Delta \mu x$) of ca. 0.5 for 2% Au on alumina. The Au catalysts were reduced at 175–250 °C for 1 h in 4% H_2/He (Pt catalysts were reduced at 250 °C for 1 h) in a continuous-flow EXAFS reactor cell (18″ long, 0.75″ i.d.) fitted at both ends with polyimid windows and valves to isolate the reactor from the atmosphere. The spectra were obtained at room temperature in the presence of H_2. The reduced Au catalysts were oxidized with flowing air at room temperature or higher (up to 225 °C), and the EXAFS spectra were obtained at room temperature in air. Pt catalysts and Au supported on alumina and silica were obtained in transmission. Depending on the loading, Au supported on titania, zirconia, ceria, and niobia were taken in transmission or fluorescence.

Phase shifts, backscattering amplitudes, and XANES references were obtained from reference compounds: $HAuCl_4$ (Aldrich) for Au^{III}–Cl, $Au(OH)_3$ (Aldrich) for Au^{III}–O, Au foil for Au^0 and Au–Au, and Pt foil for Pt–Pt. The Au XANES fits of the normalized spectra were done by a linear combination of experimental standards. Standard procedures based on WINXAS97 software were used to extract the EXAFS data. The coordination parameters were obtained by a least squares fit in q- and r-spaces of the isolated nearest-neighbor, k^2-weighted Fourier transform data. The data were also fit with both k^1 and k^3 weightings, with similar results.

3. Results

3.1. Pt catalysts

The method of catalyst preparation (including the support type, metal salt, method and pH of salt addition, drying temperature, etc.) affects the dispersion of the reduced catalyst. Pt on silica and alumina with differing dispersions were prepared by DI of $Pt(NH_3)_4(NO_3)_2$ (PTA), also called incipient wetness impregnation, or by SEA [67,70,71]. After PTA was added to the support, the catalysts were further subjected to drying or calcination at 100–625 °C. After reduction at 250 °C, the catalysts were fully reduced, and the percent dispersion of the reduced catalysts was determined by hydrogen chemisorption. These values were between 10 and 100% (see Table 1).

On silica, SEA gives catalysts with higher dispersion than DI [67]. Catalysts with the dispersions near 100% were obtained by SEA and calcined below 225 °C. As the calcination temperature increased, the dispersion decreased; for example, SEA of PTA on silica (Pt-Si12) and calcined at 550 °C gave a dispersion of 19%. DI of PTA on alumina gave catalysts with higher dispersion than those on silica. For example, calcination of PTA at about 500 °C gave dispersions of 81% on alumina (Pt-Al2) and 24% on silica (Pt-Si6). Calcination of PTA on alumina above 500 °C led to a rapid loss in dispersion, ca. 20% at 625 °C in Pt-Al7. The calcination temperature of the alumina before the addition of PTA also slightly affected Pt dispersion; for example, DI of PTA on alumina calcined at 700 °C, Pt-Al4, gave a lower dispersion (70%) that on alumina calcined at 500 °C, Pt-Al2 (80%).

EXAFS data were collected at room temperature for Pt catalysts reduced in hydrogen at 250 °C. For the smallest metallic particles, the data quality was good to about 14 $Å^{-1}$, whereas for large particles, the data were excellent at >16 $Å^{-1}$. The isolated first-shell EXAFS was obtained by a Fourier transform of the k^2-weighted data from 2.8 to 13.3 $Å^{-1}$, followed by an inverse Fourier transform from 1.4 to 2.8 Å. The model fit parameters were determined by fitting the real and imaginary parts of the Fourier transform of the isolated k^2-weighted Pt–Pt EXAFS and are summarized in Table 3. In the initial fits, all model parameters were allowed to vary to obtain the best fit. For most catalysts, as the dispersion decreased, there was a corresponding increase in the Pt–Pt coordination number (or $N_{Pt–Pt}$); however, for a few catalysts, the $N_{Pt–Pt}$ was slightly out of line with this expected trend. In general, the fits were excellent, except for small errors at the end of the data range due to truncation errors introduced during the Fourier filtering procedure. Rectangular windowing functions were used in the Fourier filtering procedure. The sensitivity of the fits was determined by fixing one model fit parameter and determining the remaining values independently. The effect of small changes in the fixed parameter on the other coordination parameters was then evaluated. These variations were determined for fits in both q- and r-spaces and with different k-weightings. The fit values of R and E_0 did not change significantly with changes in the data range, data weighting, or the other fitting parameters. Because the coordination number (CN) is correlated with the Debye–Waller factor (DWF) [72], small changes in the DWF produced small changes in the CN with no significant change in the quality of the fit. The improvement in fit was primarily at the high-k end of the data range. Thus, truncation errors led to variations in the DWF that led to slightly different $N_{Pt–Pt}$. To compare the relative $N_{Pt–Pt}$ values, the difference in DWF between the reference and the samples was fixed at 0.001 $Å^2$, similar to that found for most of the fits. With a fixed DWF, for all catalysts, $N_{Pt–Pt}$ increased as the percent dispersion decreased (Fig. 1). The catalysts on alumina and silica fit this correlation equally well. Fig. 1 shows a linear correlation (correlation coefficient, 0.96) between log(% dispersion) and $N_{Pt–Pt}$. From this empirical correlation, the percent dispersion, or fraction of atoms exposed, can be calculated from $N_{Pt–Pt}$ as follows:

$$\log(\%\ \text{dispersion}) = -0.130\ (\pm 0.005) \times (N_{Pt–Pt}) + 2.58\ (\pm 0.04).$$

Table 3
EXAFS fit parameters for reduced 2% Pt on silica and alumina with different dispersions (k^2: Δk = 2.9–12.5 $Å^{-1}$ and Δr = 1.8–3.3 Å; DWF = 0.001 $Å^2$)

Sample ID	Support	% Dispersion	$N_{Pt–Pt}$ (±10%)	R (Å) (±0.02 Å)	E_0 (eV)
Pt-Si1	SiO_2	63	6.2	2.74	−4.4
Pt-Si2	SiO_2	51	6.8	2.75	−2.9
Pt-Si3	SiO_2	29	7.9	2.75	−3.6
Pt-Si4	SiO_2	29	8.4	2.76	−2.0
Pt-Si5	SiO_2	32	7.9	2.76	−4.7
Pt-Si6	SiO_2	24	9.4	2.77	−3.1
Pt-Si7	SiO_2	79	4.7	2.75	−4.1
Pt-Si8	SiO_2	85	4.9	2.76	−4.6
Pt-Si9	SiO_2	100	4.4	2.74	−3.0
Pt-Si10	SiO_2	41	7.1	2.76	−3.6
Pt-Si11	SiO_2	24	8.4	2.77	−1.0
Pt-Si12	SiO_2	19	10.6	2.76	−1.0
Pt-Si13	SiO_2	11	11.4	2.76	−1.1
Pt-Al1	Al_2O_3	81	5.1	2.74	−3.0
Pt-Al2	Al_2O_3	81	5.6	2.74	−2.9
Pt-Al3	Al_2O_3	82	4.8	2.73	−5.5
Pt-Al4	Al_2O_3	70	5.3	2.75	−4.2
Pt-Al5	Al_2O_3	57	5.7	2.74	−4.3
Pt-Al6	Al_2O_3	30	8.4	2.76	−2.8
Pt-Al7	Al_2O_3	18	9.6	2.77	−2.4

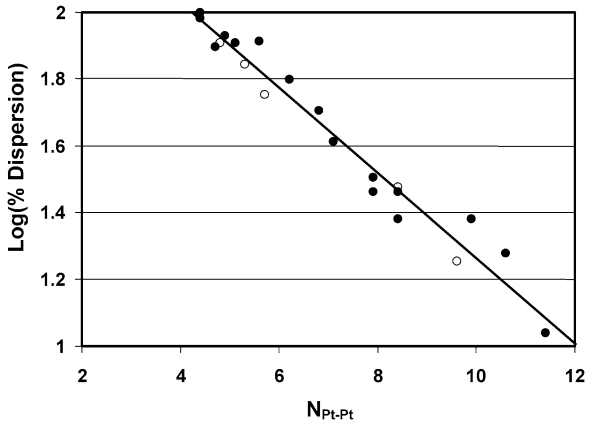

Fig. 1. Correlation between $N_{Pt–Pt}$ and the log(% dispersion) determined by hydrogen chemisorption; (●) 2% Pt on silica; (○) 2% Pt on alumina.

Table 4
EXAFS fit parameters for reduced Au catalyst (k^2: $\Delta k = 2.8$–12.4 Å^{-1} and $\Delta r = 1.7$–3.3 Å; DWF = 0.001 Å^2)

Sample ID	Support	$N_{Au–Au}$ (±10%)	R (Å) (±0.02 Å)	E_0 (eV)	%Au dispersion (Calculated)
Au-Si1	SiO_2	9.1	2.85	−3.7	24
Au-Si2	SiO_2	8.7	2.85	−4.1	27
Au-Al1	Al_2O_3	8.9	2.86	−3.5	25
Au-Al2	Al_2O_3	7.1	2.83	−3.9	44
Au-Al3	Al_2O_3	3.9	2.73	−5.9	100
Au-Al4	Al_2O_3	4.2	2.72	−8.0	100
Au-Al5	Al_2O_3	3.6	2.72	−7.7	100
Au-Al6	Al_2O_3	9.5	2.86	−3.0	21
Au-Al7	Al_2O_3	6.4	2.80	−4.4	54
Au-Ti1	TiO_2	7.6	2.82	−5.1	38
Au-Ti2	TiO_2	8.9	2.85	−3.9	25
Au-Ti3	TiO_2	9.5	2.85	−4.1	21
Au-Ti4	TiO_2	10.9	2.87	−2.7	14
Au-Ti5	TiO_2	6.3	2.81	−4.2	56
Au-Ti6	TiO_2	7.1	2.82	−4.0	44
Au-Ti7	TiO_2	12.0	2.88	−3.0	<1
Au-Ti8	TiO_2	9.7	2.86	−3.2	20
Au-Ti9	TiO_2	10.6	2.86	−3.4	15
Au-Ce1	CeO_2	5.5	2.78	−7.6	71
Au-Ce2	CeO_2	8.4	2.84	−3.7	29
Au-Ce3	CeO_2	7.9	2.83	−4.5	34
Au-Nb1	Nb_2O_5	4.9	2.77	−5.9	85
Au-Nb2	Nb_2O_5	7.2	2.83	−3.9	42
Au-Zr1	ZrO_2	6.4	2.80	−6.1	54

3.2. Au catalysts

3.2.1. Evaluation of the Au–Au bond length and gold dispersion

$HAuCl_4$ was deposited on silica, alumina, titania, ceria, niobia, and zirconia by several methods. For most catalysts, the residual Cl was removed by washing with NaOH, NH_4OH, or water. Fully reduced Au particles were obtained by reduction in H_2 at 250 °C; reduction to metallic Au occurred at about 50 °C lower on titania, silica, and niobia. EXAFS data were obtained on the reduced catalysts; the analysis procedure was identical to that for the Pt catalysts. The fit parameters for the Au catalysts are given in Table 4. As with Pt, the relative DWF was held constant at +0.001 Å^2, and the other parameters were determined independently.

Fig. 2 shows the correlation between the Au–Au CN (or $N_{Au–Au}$) and the Au–Au bond distance. As $N_{Au–Au}$ decreased, a significant decrease in the metallic bond length occurred. All Au catalysts fit the correlation equally well independent of the support type, method of preparation, Au loading, presence of Cl, and other preparation variables. Fig. 3 shows the magnitude and imaginary component of the k^2-weighted Fourier transform for Au on silica (Au-Si1) and alumina (Au-Al5) with $N_{Au–Au}$ equal to 9.1 and 3.6, respectively. As the size of the Au particles decreased, the magnitude became smaller, and the zero crossing of the imaginary component of the FT between 2.3 to 3.0 Å shifted to lower R. The Au–Au bond length ($R_{Au–Au}$) decreased from 2.85 and 2.72 Å for Au on silica and alumina, respectively. The bond length in Au foil was 2.88 Å.

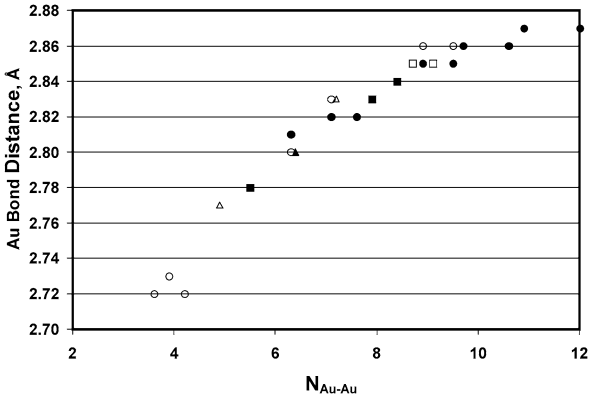

Fig. 2. Correlation between the $N_{Au–Au}$ and the Au–Au bond length Au on TiO_2 (●); Au on Al_2O_3 (○); Au on CeO_2 (■); Au on SiO_2 (□); Au on ZrO_2 (▲) and Au on Nb_2O_5 (△).

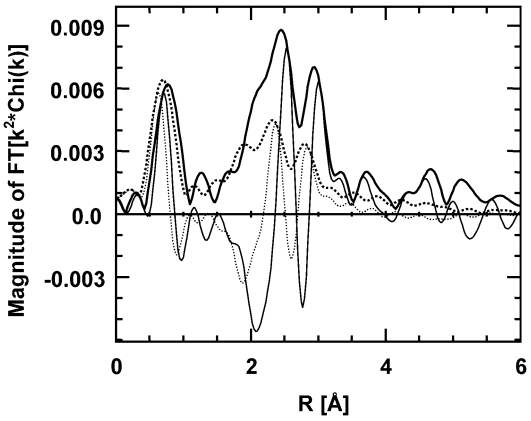

Fig. 3. Magnitude and imaginary component of the Fourier transform (k^2: $\Delta k = 2.80$–12.5 Å^{-1}). (—,—) 2.4% Au on SiO_2 (Au-Si1, $N_{Au–Au} = 9.1$, $R = 2.85$ Å). (•••, ···) 1.31% Au (20 ppm Cl) on Al_2O_3 (Au-Al5, $N_{Au–Au} = 3.6$, $R = 2.72$ Å).

Assuming that small Au and Pt particles have similar structures (both are FCC metals), from $N_{Au–Au}$, the percent dispersion of the Au catalysts can be calculated based on the Pt correlation. These estimated dispersions are also given in Table 4. As the dispersions increased above about 30%, a noticeable contraction in the metallic bond length occurred. For the smallest particles, the contraction was about 0.16 Å, or about 5.5%.

3.2.2. Reactivity of the gold clusters to oxygen

The reactivity of the Au particles toward oxidation was evaluated by XANES and EXAFS after exposure to air at room temperature and above. The fits of the XANES and EXAFS spectra for several oxidized catalysts are given in Table 5. The reactivity to air depends on the dispersion and the presence of Cl. For catalysts that contain Cl, there were no Au–Cl bonds in the EXAFS spectra of the reduced catalysts; therefore, the Cl must have been located on the support.

Fig. 4 shows the XANES spectra of small Au particles of 1.31% Au/alumina (20 ppm Cl) (Au-Al5; CN = 3.6, dispersion = 100%) and oxidized with air at room temperature and

Table 5
EXAFS fit parameters for reduced Au catalyst followed by oxidation by air (k^2: $\Delta k = 2.8$–12.4 Å^{-1} and $\Delta r = 1.7$–3.3 Å)

Sample ID (%dispersion)	Catalyst	Oxidation temperature	Fraction Au^{III}	Fraction Au^0	Scattering path	N (±10%)[a]	R (Å) (±0.02 Å)	DWF ($\times 10^{-3}$)	E_0 (eV)
Au-Si2	3.2% Au, SiO_2	None	–	1.0	Au–Au	8.7	2.85	1.0	−4.1
(27%)	3.2% Au, SiO_2	RT	–	1.0	Au–Au	9.6	2.85	1.0	−3.0
	3.2% Au, SiO_2	RT			Au–Au	−1.0(2)	2.88	1.0	−3.0
	Difference fit								
Au-Al1	0.9% Au	None	–	1.0	Au–Au	8.9	2.86	1.0	−3.5
(25%)	Al_2O_3 (1.7% Cl)								
	0.9% Au	RT	0.05	0.95	Au–Cl	0.4(5)	2.28	−2.0	2.0
	Al_2O_3 (1.7% Cl)				Au–Au	8.0	2.86	1.0	−4.1
	0.9% Au	RT			Au–Cl	−0.3(1)	2.28	−2.0	1.1
	Al_2O_3 (1.7% Cl)				Au–Au	1.1(2)	2.81	1.0	−3.5
	Difference fit								
Au-Al2	1.4% Au	None	–	1.0	Au–Au	7.1	2.84	1.0	−3.9
(44%)	Al_2O_3 (0.9% Cl)								
	1.4% Au	RT	–	1.0	Au–Au	7.5	2.86	1.0	−3.2
	Al_2O_3 (0.9% Cl)								
	1.4% Au	225 °C	–	1.0	Au–Au	8.0	2.86	1.0	−3.9
	Al_2O_3 (0.9% Cl)								
Au-Al3	0.6% Au, Al_2O_3	None	–	1.0	Au–Au	3.9	2.73	1.0	−5.9
(100%)	0.6% Au, Al_2O_3	RT	0.10	0.90	Au–O	0.3(4)	2.04	−2.0	−1.0
					Au–Au	3.8	2.74	1.0	−6.5
	0.6% Au, Al_2O_3	RT			Au–O	−0.2(2)	2.03	1.0	−1.8
	Difference fit				Au–Au	0.9(2)	2.73	1.0	−2.8
	0.6% Au, Al_2O_3	100 °C	0.10	0.90	Au–O	0.3(4)	2.04	−2.0	−1.0
					Au–Au	3.8	2.74	1.0	−6.7
	0.6% Au, Al_2O_3	100 °C			Au–O	−0.2	2.03	1.0	−2.2
	Difference fit				Au–Au	1.0	2.74	1.0	−1.5
Au-Al5	1.3% Au, Al_2O_3	None	–	1.0	Au–Au	3.6	2.72	1.0	−7.7
(100%)	1.3% Au, Al_2O_3	RT	0.10	0.90	Au–O	0.3(4)	2.04	−2.0	−1.3
					Au–Au	3.3	2.72	1.0	−7.1
	1.3% Au, Al_2O_3	RT			Au–O	−0.2(1)	2.04	−2.0	−1.5
	Difference fit				Au–Au	0.4(1)	2.72	1.0	−2.9
	1.3% Au, Al_2O_3	225 °C	0.15	0.85	Au–O	0.5(4)	2.04	−2.0	0.3
					Au–Au	2.7	2.71	1.0	−8.5
	1.3% Au, Al_2O_3	225 °C			Au–O	−0.3(1)	2.04	−2.0	−1.3
	Difference fit				Au–Au	1.0(2)	2.72	1.0	−3.0
Au-Ti1	2.9% Au, TiO_2	None	–	1.0	Au–Au	7.6	2.82	1.0	−5.1
(38%)	2.9% Au, TiO_2	RT	0.05	0.95	Au–O	0.3(5)	2.04	1.0	0.5
					Au–Au	8.5	2.83	1.0	−3.7
	2.9% Au, TiO_2	RT			Au–O	−0.2(1)	2.05	−0.5	−1.1
	Difference fit				Au–Au	−0.7(2)	2.88	−3.0	−2.7
Au-Ti3	3.3% Au, TiO_2	None	–	1.0	Au–Au	9.5	2.85	1.0	−3.9
(21%)	3.3% Au, TiO_2	RT	–	1.0	Au–Au	10.5	2.87	1.0	−4.0
	3.3% Au, TiO_2	RT			Au–Au	−1.1(2)	2.88	−1.0	−4.2
	Difference fit								

[a] Unless marked otherwise.

225 °C. On contact with air at room temperature, a small increase in the white line intensity occurred, indicating partial oxidation of the metallic Au. Although the dispersion of the reduced catalyst was near 100%, only about 10% of the Au atoms were oxidized at room temperature. At higher temperatures, an additional small increase in Au oxidation occurred. The magnitude of the k^2-weighted Fourier transforms of the reduced and oxidized 1.31% Au/alumina (20 ppm Cl) catalysts, Au-Al5, are given in Fig. 5. In the reduced catalyst, the peaks from about 1.5 to 3.0 Å are due to scattering from Au atoms at 2.72 Å. Oxidation led to a small decrease in the intensity of the metallic Au peaks, with the addition of a small feature at about 1.8 Å due to an oxygen contribution. Increasing the oxidation temperature led to an additional decrease in the size of the metallic Au peaks and a further increase in intensity of the Au–O contribution. After oxidation at 225 °C, about 15% of the metallic Au was oxidized. On small Au particles on titania [i.e., 2.9% Au prepared by deposition precipitation with NaOH (Au-Ti1; $N_{Au-Au} = 7.6$, dispersion = 54%, $R = 2.80$ Å)], air oxidation at room temperature led to the formation of a small amount

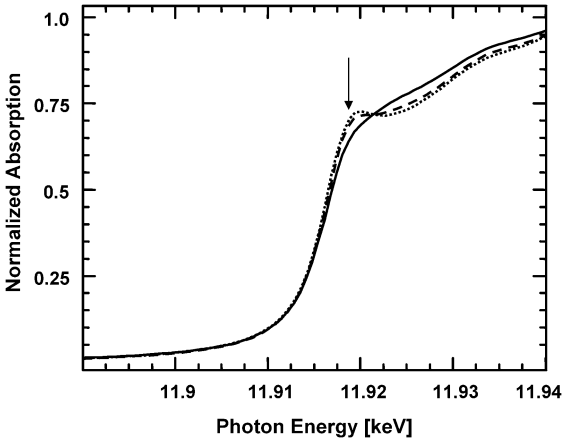

Fig. 4. Au XANES (11.87–11.95 keV) for 1.31% Au/alumina (20 ppm Cl), Au-Al5. (—) Reduced in H_2 at 250 °C ($N_{Au–Au} = 3.6$ and $R = 2.72$ Å). (- - -) Reduced followed by air at RT ($Au^{III} = 0.10$ and $Au^0 = 0.90$). (···) Reduced followed by air at 225 °C ($Au^{III} = 0.15$ and $Au^0 = 0.85$).

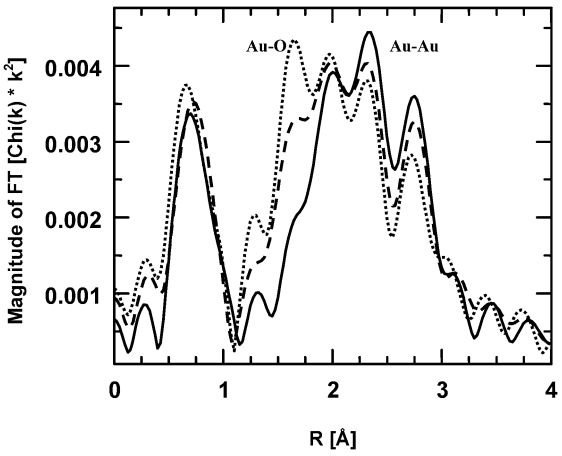

Fig. 5. k^2-Weighted magnitude of Fourier transform of 1.31% Au/alumina (20 ppm Cl), Au-Al5 (k^2: $\Delta k = 3.05$–13.5 Å^{-1}). (—) Reduced in H_2 at 250 °C ($N_{Au–Au} = 3.6$ and $R = 2.72$ Å). (- - -) Reduced followed by air at RT ($N_{Au–Au} = 3.3$ and $N_{Au–O} = 0.3$). (···) Reduced followed by air at 225 °C ($N_{Au–Au} = 2.7$ and $N_{Au–O} = 0.4$).

of oxidized gold similar to that on small Au particles on alumina. Unlike alumina, however, the metallic particles on titania sintered slightly ($N_{Au–Au}$ increased to 8.5; see Table 5). In the oxidized catalyst, about 95% of the Au is metallic; thus the true $N_{Au–Au}$ is 8.9 (8.5/0.95). From the correlation in Eq. (1), on exposure to room temperature air, the dispersion decreased to about 25%. Consistent with the increase in the CN, the bond length increased to 2.83 Å in the oxidized catalyst.

Because the Au–O peaks are small and overlap with the larger Au–Au contribution, independent determination of all model fit parameters for the former was not possible. In the direct fits of the air-oxidized catalyst, the $N_{Au–O}$ was determined by fixing R, DWF, and E_0 to values determined for the nonreduced, Cl-free catalyst precursor. EXAFS and XANES analysis of (nonreduced) Au/TiO_2 and Au/Al_2O_3 catalysts prepared by deposition-precipitation with NaOH or urea for removal of Cl indicate that Au is present as Au^{III} oxide with four Au–O bonds

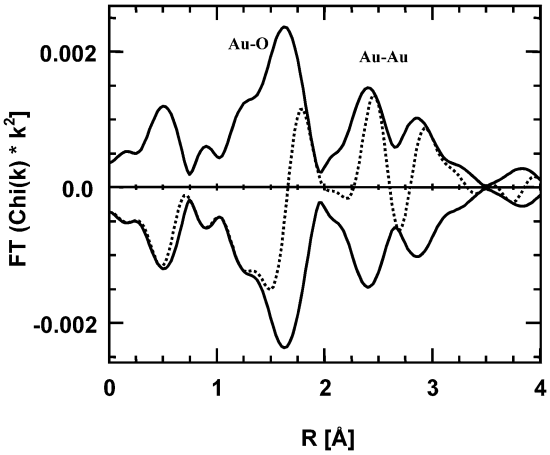

Fig. 6. EXAFS of the difference file for 1.31% Au/alumina (20 ppm Cl), Au-Al5, reduced at 250 °C followed by air at 225 °C (k^2: $\Delta k = 3.05$–12.8 Å^{-1}). (—) Fourier transform magnitude. (- - -) Imaginary component of the Fourier transform (Au–O is 180° out of phase).

at 2.03 Å [27,73]. These fit parameters were assumed for the Au–O contribution in the direct fits of the air-oxidized catalysts. The $N_{Au–O}$ estimates for 1.31% Au/alumina (20 ppm Cl), Au-Al5, were 0.3 and 0.5 for oxidation at room temperature and 225 °C, respectively. These values are in line with the fraction of Au^{III} determined by XANES assuming that oxidized gold has four Au–O bonds. A more reliable method for determining the small Au–O contribution is possible by analyzing the difference spectrum, that is, subtracting the oxidized EXAFS spectrum from the reduced spectrum [74]. In the difference spectrum, Au species that are unchanged are subtracted and are not present in the difference spectrum. Scattering paths present in the oxidized spectrum but not in the reduced spectrum are 180° out of phase with the reference file (e.g., Au–O). By isolating only the small differences between spectra, it is sometimes possible to fit a very small component of the total EXAFS signal with better confidence in the results, because the statistically determined errors can be substantially reduced.

Fig. 6 shows the Fourier transform of the difference spectrum of 1.31% Au on Alumina (20 ppm Cl), Au-Al5, reduced and subsequently oxidized at 225 °C. Oxidation of the reduced catalyst at 225 °C led to the formation of a small number of Au–O bonds and the loss of small number of Au–Au bonds. The model fit parameters of the peaks in the difference spectrum are also given in Table 5; the results are consistent with those for the direct fits. In fitting the difference spectrum R, DWF, and E_0 were not fixed as they were in the direct fits.

For catalysts with moderate-sized Au particles (dispersions of about 25–50%) without Cl or with low Cl levels, exposure to air led to particle growth without formation of oxidized Au. Fig. 7 shows the XANES for 3.2% Au on silica (Au-Si2) reduced at 175 °C (dispersion = 0.27) and air oxidized at room temperature. After oxidation, there is no indication that the metallic Au was oxidized. Although the XANES results indicate little change, from the magnitude of the FT it is apparent that the size of the metallic particles increased slightly

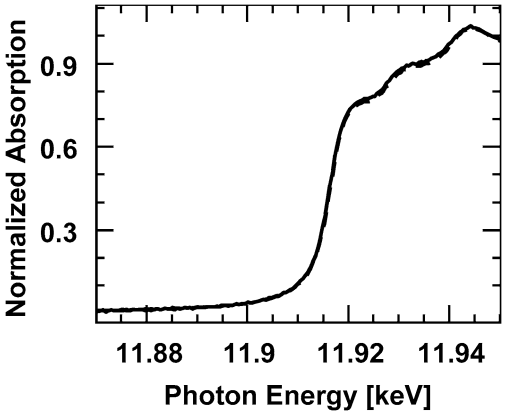

Fig. 7. Au XANES (11.87–11.95 keV) for 3.2% Au/silica, Au-Si2. (—) Reduced in H_2 at 250 °C ($Au^0 = 1.00$). (- - -) Reduced followed by air at RT ($Au^0 = 1.00$).

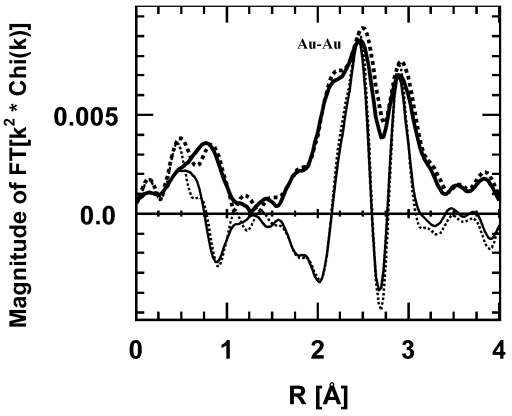

Fig. 8. k^2-Weighted magnitude and imaginary component of Fourier transform of 3.2% Au on silica, Au-Si2 (k^2: $\Delta k = 2.6$–13.4 Å^{-1}). (—, —) Reduced in H_2 at 250 °C ($N_{Au–Au} = 8.7$ and $R = 2.85$ Å). (•••, ···) Reduced followed by air at RT ($N_{Au–Au} = 9.6$ and $R = 2.85$ Å).

(Fig. 8). Specifically, for Au on silica, exposure to room temperature air increased the $N_{Au–Au}$ from 8.7 to 9.6, or decreased the estimated dispersion from about 30 to 20%. Similar results were observed for 1.4% Au on alumina with 0.9% Cl, Au-Al2. $N_{Au–Au}$ increased from 7.1 for the reduced catalyst to 7.5 for air at room temperature and 8.0 for air at 175 °C, corresponding to changes in the dispersions of about 45, 40, and 35%, respectively. Sintering of the Au particles on exposure to room temperature air was similar to that reported previously for 25-Å Au particles supported on TiO_2(110) thin films [75–77].

For Au catalysts with high levels of Cl on the support, Au-Al1, oxidation may also lead to the formation of Au–Cl bonds [73]. Exposure to air at room temperature of metallic Au on alumina with 1.7% Cl led to the formation of a small number of Au^{III}–Cl bonds, but no Au–O bonds. The presence of the Au–Cl coordination is clearly apparent in the difference spectrum in Fig. 9. The fit identifies this feature as Au–Cl (the imaginary component of the FT is 180° out of phase from the Au–Cl reference spectrum), not Au–O. As with Cl-free catalysts, only about 10% of the metallic Au nanoparticles were oxidized.

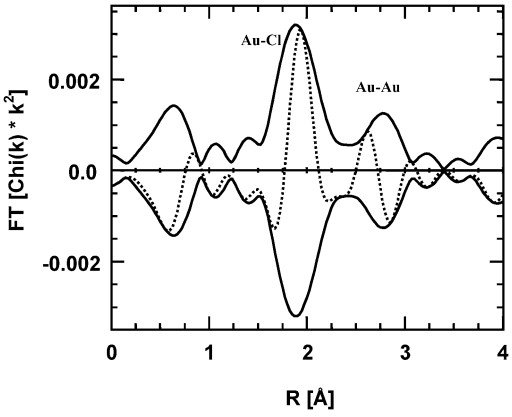

Fig. 9. EXAFS of the difference file for 0.9% Au/alumina (1.7% Cl), Au-Al1, reduced at 250 °C followed by air at RT (k^2: $\Delta k = 3.05$–12.8 Å^{-1}). (—) Fourier transform magnitude. (- - -) Imaginary component of the Fourier transform (Au–Cl is 180° out of phase).

4. Discussion

Although contractions in the bond distance in small unsupported (and on weakly interacting supported) metal particles may be up to about 0.2 Å, for oxide-supported metal particles the contraction in the interatomic distance is generally much smaller. Bond distances of Os, Ir, and Pt catalysts measured in H_2 with dispersions near 1.0 on silica and alumina display a contraction in bond length of only about 0.03 Å [78–80]. A similar contraction in the Pt–Pt bond distance (measured in the presence of chemisorbed H_2) was observed for the Pt catalysts in this study (Table 3). Under vacuum, however, a contraction of the bond distance of up to about 0.09 Å has been observed for highly dispersed Pt [53]. Previously reported Au catalysts on alumina, titania, and magnesia have bond lengths of about 2.85 Å, compared with 2.88 Å for Au foil [81–83]; however, theoretical calculations of small Pt and Au clusters predict a shortening of the metal–metal distance with decreasing cluster size. Gold dimers, trimers, and hexamers are expected to have a bond lengths of 2.58, 2.64, and 2.77 Å, respectively [84]. Moreover, theory predicts different Au–Au distances for linear, planar, and three-dimensional structures [85].

In this study, for Au catalysts with dispersion <30%, small changes in the bond length occurred. However, for catalysts with dispersion >30%, the contraction of the Au bond distance was significantly larger (e.g., about 0.15 Å for catalysts with near-100% dispersion). The Au particle size may be estimated using a previously reported correlation between the coordination number and the particle size [86,87]. Fig. 10 compares the Au–Au bond lengths and particle sizes; it includes particle size and bond lengths for previously reported unsupported Au particles [48,49,51]. There is a noticeable decrease in the bond length for particles smaller than about 30 Å, whereas particles larger than about 40 Å show only minor changes from those in Au foil. The similarity in bond length with particle size in supported and unsupported particles suggests that the support has a minimal effect on the length of the Au bond.

A decrease in particle size is also accompanied by a change in the electronic properties of metal nanoparticles [13,17,88–

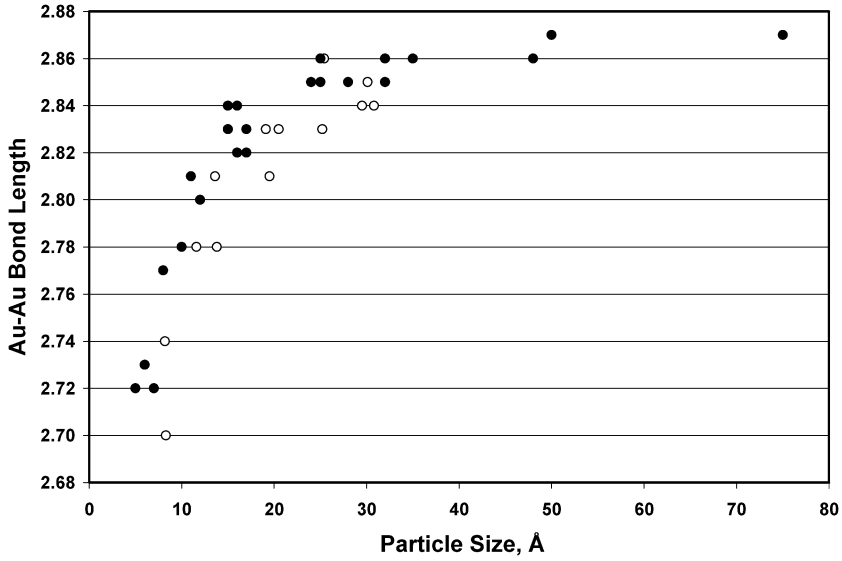

Fig. 10. Comparison of the bond length in unsupported (○) [48,50] and supported (●) Au nanoparticles (this study). Metal particle size for the catalysts was determined from a correlation between the Au bond length and particle size [85,86].

90]. Several recent reviews have summarized the evidence for changes in the electronic properties of small Au particles [13,17]. Because the contraction of the metallic bond distance for unsupported Au is very similar to that in the catalysts given in this paper, the changes in the electronic properties of these small particles would be expected to be similar to those observed for unsupported particles and thin films. STS on two-dimensional Au particles deposited on TiO_2(110) has shown that the onset of catalytic activity coincides with detection of a band gap of 0.2–0.6 eV for 32-Å particles [23]. A maximum band gap of 1.4 eV was observed for particles smaller than 20 Å. A similar transition in the band gap was observed for 10-Å Au particles on graphitic carbon [91]. For Au particles smaller than 30 Å on diamond, field emission spectroscopy has shown discrete electron states rather than a continuum, as present in bulk gold [92]. XPS has also been used to study electronic effects in small gold catalysts. Positive binding energies for small gold particles on silica and carbon were interpreted as resulting from rehybridization of the valence orbitals [93]. A similar shift in band and degree of d-band splitting position was observed for small Au particles on aluminum and alumina [94]. Because these changes were the same on both supports, the changes were thought to be due to the electronic properties of small particles. Changes in the d-band splitting of Au on carbon occurred for particles of about 19 Å[95]. Similar changes in electronic properties for 20-Å Au particles on Ti(110) were detected by HREELS [96].

Theoretical calculations on gold clusters of increasing size indicate that with increasing cluster size, 6s–5d orbital rehybridization is enhanced [84,85]. Increasing the number of atoms in a cluster increases the width of the s- (and p-) and d-bands, increasing their overlap with a decrease in the band gap. The shorter Au–Au distance in small particles favors enhanced d–d interactions, narrowing the d-band and lowering the energy of the d-orbitals. The ideal electron configuration of gold is $5d^{10}6s^{1}$; however, because of rehybridization, larger clusters

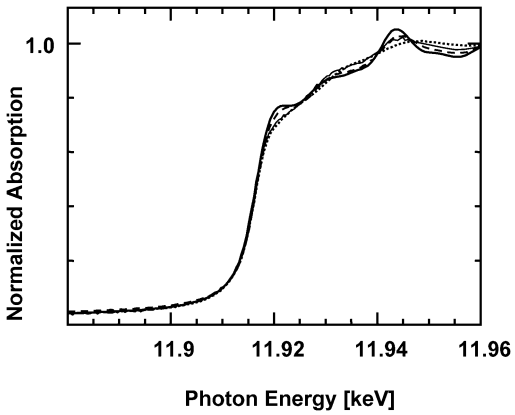

Fig. 11. Au XANES spectra for different particle size (11.88–11.96 keV). (—) Au foil ($N_{Au–Au} = 12.0$, $R = 2.88$ Å). (- - -) 2.4% Au on SiO_2 (Au-Si1, $N_{Au–Au} = 9.1$, $R = 2.85$ Å). (—) 3.0% Au on TiO_2 (Au-Ti1, $N_{Au–Au} = 7.6$, $R = 2.82$ Å). (···) 1.3% Au on alumina (Au-Al3, $N_{Au–Au} = 3.9$, $R = 2.72$ Å).

have an electron configuration of $5d^{10-x}6s^{1+x}$, with the d-band density of states closer to the Fermi level and increased holes in the d-band [97]. Evidence of a decrease in d-orbital occupancy in smaller particles was observed in our XANES spectra (Fig. 11). As the particle size decreases, there is a decrease in the white line (the first feature above the rising edge) [98]. The decrease in the white line with decreasing particle size of the Au catalysts is also consistent with theoretical calculations that predict a decrease in the intensity of the white line in small particles [99,100].

4.1. Reactivity of gold clusters to oxygen

A review of the adsorptive properties indicates that Au foil weakly chemisorbs CO but is unable to dissociate or molecularly adsorb H_2 and O_2 [17,101,102]. For example, after H_2 reduction, the IR spectrum of CO on 30-Å gold particles supported on MgO indicates linear absorption at 2085 cm^{-1}

[103]. After reduction of Au nanoparticles on TiO_2, two IR bands at 2055 and 1990 cm^{-1} have been attributed to CO adsorbed on small Au clusters [104]. However, few studies have demonstrated that supported gold nanoparticles adsorb or react with O_2. For example, volumetric oxygen adsorption on reduced gold particles on SiO_2 and MgO displayed a maximum uptake of molecular O_2 at 200 °C [105]. More recently, oxygen adsorption and hydrogen pulse titration of chemisorbed oxygen was used to determine the dispersion of gold on Au/Al_2O_3 [106]. In both cases, assuming a stoichiometry of gold-to-O_2 ratio of two, there was good agreement between the average gold particle size determined by oxygen chemisorption and TEM.

TOF-SIMS spectra of Au/TiO_2 and Au/Al_2O_3 calcined at 350 °C have indicated that gold particles were not fully reduced. The presence of AuO^- and $AuO_2{}^-$ ion clusters is consistent with either chemisorbed oxygen or partially oxidized metallic gold [107]; however, because the samples were transferred in ambient air before the analysis, the small Au particles (20–50 Å) may have been reoxidized by contact with air. Field ion microscopy images of a 500-Å-diameter Au(111) crystal tip in contact with air at 25–180 °C indicated oxidation of the surface [108]. Finally, temperature-programmed oxidation of 30 Å metallic gold particles supported on MgO were thought to be completely oxidized at high temperature [83]; however, no other studies have indicated such a high degree of oxidation of Au nanoparticles.

In this study, for the smallest particles, approximately 10% of the atoms were oxidized on exposure to air at room temperature and above, whereas large particles were not. EXAFS and XANES indicate that oxidation with the formation of Au^{III} and O^{2-} occurred rather than chemisorption of atomic oxygen on metallic Au atoms. This suggests that the reactivity of gold nanoparticles for CO oxidation might result from the surface oxidation of gold atoms, followed by reduction with CO (Eley–Rideal or Langmuir–Hinshelwood mechanism) and formation of CO_2 [104]. Therefore, catalytic activity will be determined by the rates of Au^0 oxidation and Au^{III} reduction by CO. Under reaction conditions, both CO and O_2 are present. XANES spectra indicate that Au^{III} is readily reduced in the presence of CO and O_2 [109,110]. In addition, under reaction conditions, little oxidized Au is observed [111], suggesting that under steady-state conditions, the fraction of oxidized surface atoms is small and that the rate of surface oxidation may be rate-limiting.

We conclude that the change in the chemisorption and reaction properties in small metallic Au particles results from a change in the rehybridization of the s–p–d valence orbitals, leading to increased d-electron density and widening of the s–p to d orbital band gap compared with large particles. Although this and other studies indicate that the catalytic activity of Au is dependent on the formation of small particles (especially those smaller than about 30 Å), other effects, including interaction with the support and activation of oxygen by the support, also may be important. To establish the effect of the support on the activity, it will be necessary to prepare particles of identical size on different supports and compare the rates. For Au nanoparticles of nearly identical size, the temperature to obtain 50% CO conversion decreases in the order $TiO_2 < ZrO_2 < Al_2O_3$ [112], which generally parallels the ease of gold oxide reduction. Thus, low-temperature oxidation activity may be related to the ease of gold reduction, which seems to be affected by the support. However, more detailed studies are needed to establish the role of the support in the CO oxidation activity of Au nanoparticles.

5. Conclusion

A correlation between the percent dispersion of Pt catalysts determined by hydrogen chemisorption and the N_{Pt-Pt} has been established and used to determine the dispersion of fully reduced Au nanoparticles. As the dispersion of the Au catalysts increases, a contraction of the Au–Au bond length occurs. The Au–Au contraction is independent of the type of support and similar to that previously reported for unsupported Au particles. Using a literature correlation, the Au particle size was estimated from N_{Au-Au}. For particles larger than about 40 Å, there is little change in the metallic bond length, whereas in catalysts with dispersions near 100% (ca. 10 Å), the contraction is about 0.15 Å. Besides a contraction in the Au bond distance with decreasing particle size, a decrease in the intensity of the white line of the XANES spectrum also occurs. This decreased white line intensity is consistent with an increase in the s–p to d band gap and increased d-electron density in small particles. Au particles smaller than about 30 Å are also reactive to air, leading to oxidation of about 10% of the Au atoms, whereas larger particles are not oxidized. It is suggested that the high oxidation activity of Au nanoparticles is due to reduction of oxidized Au atoms by CO, forming CO_2.

Acknowledgments

C.L., L.D., and J.T.M. gratefully acknowledge the World Gold Council's Gold Research Opportunities Worldwide (GROW) grant; J.R.R. gratefully acknowledges the support of the National Science Foundation (grant CTS-0243210); and E.B. and J.A.v.B. acknowledge the Swiss National Science Foundation for partial funding of this work (Nr. 2-77264-03). Use of the Advanced Photon Source was supported by the U.S. Department of Energy, Office of Science, Office of Basic Energy Sciences (contract W-31-109-Eng-38). MR-CAT operations are supported by the Department of Energy and member institutions. Further support from the National Science Foundation (grant CTS-9908181) is also gratefully acknowledged.

References

[1] G.C. Bond, Gold Bull. 5 (1972) 11.
[2] J. Schwank, Gold Bull. 16 (4) (1983) 103.
[3] G.J. Hutchings, Gold Bull. 29 (4) (1996) 123.
[4] D. Thompson, Prec. Met. 22 (1998) 269.
[5] D. Thompson, Gold Bull. 31 (4) (1998) 111.
[6] G.C. Bond, D.T. Thompson, Catal. Rev.-Sci. Eng. 41 (3–4) (1999) 319.
[7] M. Haruta, T. Kobayashi, H. Sano, N. Yamada, Chem. Lett. 2 (1987) 405.
[8] M. Haruta, Catal. Today 36 (1997) 153.
[9] M. Haruta, Catal. Surv. Japan 1 (1997) 61.

[10] M. Haruta, 3rd World Congress on Oxidation Catalysis, Elsevier Science B.V., Amsterdam, 1997, p. 123.
[11] M. Haruta, M. Daté, Appl. Catal. A 222 (2001) 427.
[12] R.J.H. Grisel, K.-J. Weststrate, A. Gluhoi, B.E. Nieuwenhuys, Gold Bull. 35 (2002) 39.
[13] A.K. Santra, D.W. Goodman, J. Phys.: Condens. Matter 14 (2002) R31.
[14] G.J. Hutchings, Catal. Today 72 (2002) 11.
[15] M. Haruta, Chem. Record 3 (2003) 75.
[16] M. Haruta, J. New Mater. Electrochem. Syst. 7 (2004) 163.
[17] R. Meyer, C. Lemire, S.K. Shaikhutdinov, H.J. Freund, Gold Bull. 37 (2004) 72.
[18] G.J. Hutchings, Catal. Today 100 (2005) 55.
[19] M. Haruta, S. Tsubota, T. Kobayashi, H. Kageyama, M.J. Genet, B. Delmon, J. Catal. 144 (1993) 175.
[20] S. Tsubota, D.A.H. Cunningham, Y. Bando, M. Haruta, Prep. Catal. VI, Scientific Basis for the Preparation of Heterogeneous Catalysts, Elsevier Science B.V., Amsterdam, 1995, p. 277.
[21] F. Boccuzzi, A. Chiorino, S. Tsubota, M. Hurata, J. Phys. Chem. 100 (1996) 3625.
[22] G.R. Bamwenda, S. Tsubota, T. Nakamura, M. Haruta, Catal. Lett. 44 (1997) 83.
[23] M. Valden, X. Lai, D.W. Goodman, Science 281 (1998) 1647.
[24] A.I. Kozlov, A.P. Kozlova, K. Asakura, Y. Matsui, T. Kogure, T. Shido, Y. Iwasawa, J. Catal. 196 (2000) 56.
[25] P. Claus, A. Bruckner, C. Mohr, H. Hofmeister, J. Am. Chem. Soc. 122 (2000) 11430.
[26] B. Schumacher, V. Plzak, K. Kinne, R.J. Behm, Catal. Lett. (2003) 109.
[27] R. Zanella, S. Giorgio, C.-H. Shin, C.R. Henry, C. Louis, J. Catal. 222 (2004) 357.
[28] V. Schwartz, D.R. Mullins, W. Yan, B. Chen, S. Dai, S.H. Overbury, J. Phys. Chem. B 108 (40) (2004) 15782.
[29] I.N. Remediakis, N. Lopez, J.K. Nørskov, Angew. Chem. Int. Ed. 44 (2005) 1824.
[30] C.G. Bond, D.T. Thompson, Gold Bull. 33 (2000) 41.
[31] C.K. Costello, J.H. Yang, H.Y. Law, Y. Wang, J.N. Lin, L.D. Marks, M.D. Kung, H.H. Kung, Appl. Catal. A 243 (2003) 15.
[32] A. Sanchez, S. Abbet, U. Heiz, W.D. Schneider, H. Häkkinen, R.N. Barnett, U. Landman, J. Phys. Chem. A 103 (1999) 9573.
[33] B. Yoon, H. Häkkinen, U. Landman, A.S. Wörz, J.-M. Antonietti, S. Abbet, K. Judai, U. Heiz, Science 307 (2005) 40.
[34] Q. Fu, H. Saltsburg, M. Flytzani-Stephanopoulos, Science 301 (2003) 935.
[35] J. Guzman, B.C. Gates, Angew. Chem. Int. Ed. 42 (2003) 690.
[36] L.M. Molina, B. Hammer, Phys. Rev. Lett. 90 (2003) 206102.
[37] Z.-P. Liu, X.-Q. Gong, J. Kohanoff, C. Sanchez, P. Hu, Phys. Rev. Lett. 91 (2003) 266102.
[38] C.L. Cleveland, U. Landman, T.G. Schaaff, M.N. Shafigullin, P.W. Stephens, R.L. Whetten, Phys. Rev. Lett. 79 (1997) 1873.
[39] J. Uppenbrink, D.J. Wales, J. Chem. Phys. 96 (1992) 8520.
[40] M.J. Yacaman, S. Fuentes, J.M. Dominguez, Surf. Sci. 106 (1981) 472.
[41] B. Moraweck, A.J. Renouprez, Surf. Sci. 106 (1981) 35.
[42] C.R. Berry, Phys. Rev. 88 (3) (1952) 596.
[43] H.J. Wasserman, J.S. Vermaak, Surf. Sci. 22 (1970) 164.
[44] H. Purdum, P.A. Montano, G.K. Shenoy, T.I. Morrison, Phys. Rev. B 25 (7) (1982) 4412.
[45] P.A. Montano, W. Schulze, B. Tesche, G.K. Shenoy, T.I. Morrison, Phys. Rev. B 30 (1984) 672.
[46] P.A. Montano, H. Purdum, G.K. Shenoy, T.I. Morrison, Surf. Sci. 156 (1985) 228.
[47] K. Heinemann, H. Poppa, Surf. Sci. 156 (1985) 265.
[48] A. Balerna, E. Bernieri, P. Picozzi, A. Reale, S. Santucci, E. Burattini, S. Mobilio, Surf. Sci. 156 (1985) 206.
[49] A. Balerna, E. Bernieri, P. Picozzi, A. Reale, S. Santucci, E. Burattini, S. Mobilio, Phys. Rev. B 31 (8) (1985) 5058.
[50] P.A. Montano, G.K. Shenoy, E.E. Alp, W. Schulze, J. Urban, Phys. Rev. B 56 (1986) 2076.
[51] A. Pinto, A.R. Pennisi, G. Faraci, G. D'Agostino, S. Mobilio, F. Boscherini, Phys. Rev. B 51 (8) (1995) 5315.
[52] M. Klimenkov, S. Nepijko, H. Kuhlenbeck, M. Bäumer, R. Schlögl, H.-J. Freund, Surf. Sci. 391 (1997) 27.
[53] M.K. Oudenhuijzen, J.H. Bitter, D.C. Koningsberger, J. Phys. Chem. B 105 (20) (2001) 4616.
[54] P.A. Montano, J. Zhao, M. Ramanathan, G.K. Shenoy, W. Chulze, Physica B 158 (1–3) (1989) 242.
[55] G. Apai, J.F. Hamilton, J. Stöhr, A. Thompson, Phys. Rev. Lett. 43 (2) (1979) 165.
[56] M. de Crescenzi, P. Picozzi, S. Santucci, C. Battistoni, G. Mattogno, Solid State Commun. 51 (10) (1984) 811.
[57] R. Dupree, C.T. Forwood, M.J.A. Smith, Phys. Status Solidi 24 (1967) 525.
[58] R. Monot, A. Câtelain, J.P. Borel, Phys. Lett. A 34 (1971) 57.
[59] M.G. Mason, L.J. Gerenser, S.-T. Lee, Phys. Rev. Lett. 39 (5) (1977) 288.
[60] D. Schmeisser, K. Jocobi, D.M. Kolb, J. Chem. Phys. 75 (11) (1981) 5300.
[61] S.-T. Lee, G. Apai, M.G. Mason, R. Benbow, Z. Hurych, Phys. Rev. B 23 (2) (1981) 505.
[62] U. Kreibig, L. Genzel, Surf. Sci. 156 (1985) 678.
[63] G. Schmid, Chem. Rev. 92 (1992) 1709.
[64] C. Binns, Surf. Sci. Rep. 44 (2001) 1.
[65] L. Oberli, R. Monot, H.J. Mathieu, D. Landolt, J. Buttet, Surf. Sci. 106 (1981) 301.
[66] C. Lemire, R. Meyer, S.K. Shaikhutdinov, H.J. Freund, Surf. Sci. 552 (2004) 27.
[67] J.T. Miller, M. Schreier, A.J. Kropf, J.R. Regalbuto, J. Catal. 225 (2004) 203.
[68] R. Zenalla, S. Giorgio, C. Henry, C. Louis, J. Phys. Chem. B 106 (2002) 7634.
[69] R. Zenalla, L. Delannoy, C. Louis, Appl. Catal. A 291 (2005) 62.
[70] J.R. Regalbuto, M. Schreier, X. Hao, W.A. Spieker, J.G. Kim, J.T. Miller, A.J. Kropf, Studies in Surface Science and Catalysis, Preparation of Catalysts VIII, vol. 143, Elsevier Science, B.V., Amsterdam, 2002, p. 45.
[71] W.A. Spieker, J.T. Miller, A.J. Kropf, J.R. Regalbuto, Appl. Catal. A: Gen. 243 (2003) 53.
[72] B.K. Teo, EXAFS: Basic Principles and Data Analysis, Springer-Verlag, Berlin, 1986, p. 131.
[73] J.Y. Yang, J.D. Henao, C. Costello, M.C. Kung, H.H. Kung, J.T. Miller, A.J. Kropf, J.R. Regalbuto, M. Bore, H.N. Pham, A.K. Dayte, J.D. Laeger, Appl. Catal. A: Gen. 291 (2005) 73.
[74] J.T. Miller, C.L. Marshall, A.J. Kropf, J. Catal. 202 (2001) 89.
[75] X. Lai, D.W. Goodman, J. Mol. Catal. 162 (2000) 33.
[76] K. Fukui, S. Sugiyama, Y. Iwasawa, Phys. Chem. Chem. Phys. 3 (2001) 3871.
[77] E.C.H. Sykes, F.J. Williams, M.S. Tikhov, R.M. Lambert, J. Phys. Chem. B 106 (2002) 5390.
[78] G.H. Via, J.H. Sinfelt, F.W. Lytle, J. Chem. Phys. 71 (1979) 690.
[79] P. Lagarde, T. Murata, G. Vlaic, E. Freund, H. Dexpert, J.P. Bournonville, J. Catal. 84 (1983) 333.
[80] E.C. Marques, D.R. Sandstrom, F.W. Lytle, R.B. Greegor, J. Chem. Phys. 72 (1982) 1027.
[81] J. Guzman, B.C. Gates, J. Phys. Chem. B 106 (2002) 7659.
[82] J. Guzman, B.C. Gates, Langmuir 19 (2003) 3897.
[83] J. Guzman, B.C. Gates, J. Phys. Chem. B 107 (2003) 2242.
[84] P.K. Jain, Struct. Chem. 16 (2005) 421.
[85] G.H. Wang, J.J. Zhao, Phys. Rev. B 66 (2002) 35481.
[86] J. de Graaf, J. van Dillen, K.P. de Jong, D.C. Koningsberger, J. Catal. 203 (2001) 307.
[87] A.I. Frenkel, C.W. Hills, R.G. Nuzzo, J. Phys. Chem. B 105 (51) (2001) 12689.
[88] J.R. Anderson, Sci. Prog. Oxf. 69 (1985) 461.
[89] M. Che, C.O. Bennett, Adv. Catal. 36 (1989) 55.
[90] P.L.J. Gunter, J.W. Niemantsverdriet, F.H. Ribeiro, G.A. Somorjai, Catal. Rev. Sci. Eng. 39 (1977) 77.
[91] C.P. Vinod, G.U. Kulkarni, C.N.R. Rao, Chem. Phys. Lett. 289 (1998) 329.
[92] M.E. Lin, R. Reifenberger, A. Ramachandra, R.P. Andres, Phys. Rev. B 46 (1992) 15498.
[93] M.G. Mason, Phys. Rev. B 27 (1983) 748.
[94] K.S. Ling, W.R. Salaneck, I.A. Aksay, Solid State Commun. 19 (1976) 329.

[95] S.B. DiCenzo, S.D. Berry, E.H. Hartford, Phys. Rev. B 38 (1988) 8465.
[96] S.T. Lee, G. Apai, M.G. Mason, R. Benbow, Z. Hurych, Phys. Rev. B 23 (1981) 505.
[97] L.F. Mattheiss, R.E. Dietz, Phys. Rev. B 22 (1980) 1663.
[98] F.W. Lytle, P.S.P. Wei, R.B. Greegor, G.H. Via, J.H. Sinfelt, J. Phys. Chem. 70 (1979) 4849.
[99] D. Bazin, D. Sayers, J.J. Rehr, C. Motter, J. Phys. Chem. B 101 (1997) 5332.
[100] D. Bazin, J.J. Rehr, J. Phys. Chem. B 107 (2003) 12398.
[101] W.R. MacDonald, K.E. Hayes, J. Catal. 18 (1970) 115.
[102] P.C. Richardson, D.R. Rossington, J. Catal. 20 (1971) 420.
[103] J. Schwank, G. Parravano, H.L. Gruber, J. Catal. 61 (1980) 19.
[104] F. Boccuzzi, A. Chiorino, M. Manzoli, Surf. Sci. 454–456 (2000) 942.
[105] T. Fukushima, S. Galvangno, G. Parravano, J. Catal. 57 (1979) 177.
[106] H. Berndt, I. Pitsch, S. Evert, K. Struve, M.-M. Pohl, J. Radnik, A. Martin, Appl. Catal. A: Gen. 244 (2003) 169.
[107] L. Fu, N.Q. Wu, J.H. Yang, F. Qu, D.L. Johnson, M.C. Kung, H.H. Kung, V.P. David, J. Phys. Chem. B 109 (2005) 3704.
[108] T. Bar, T.V. de Bocarme, B.E. Nieuwenhuys, N. Kruse, Catal. Lett. 74 (2001) 127.
[109] J.H. Yang, J.T. Miller, J.D. Henao, Y. Wang, M. Raphulu, M.C. Kung, H.H. Kung, J. Phys. Chem. B 109 (2005) 10319.
[110] J.A. van Bokhoven, C. Louis, J.T. Miller, M. Tromp, O.V. Sofanova, P. Glatzel, Angew. Chem. Int. Ed., in press.
[111] N. Weiher, E. Bus, L. Delannoy, C. Louis, D.E. Ramaker, J.T. Miller, J.A. van Bokhoven, J. Catal. 240 (2006) 100.
[112] S. Arii, F. Mortin, A.J. Renouprez, J.L. Roussert, J. Am. Chem. Soc. 126 (2004) 1199.